Cell Reports

Article

Structure and transport mechanism of the human cholesterol transporter ABCG1

Graphical abstract

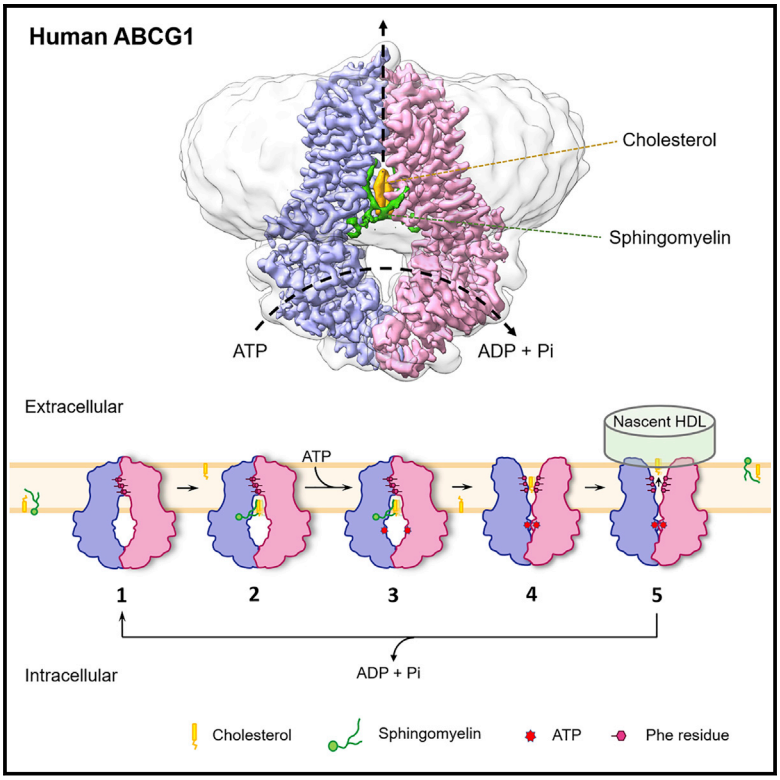

Highlights

- 3.26-Å cryo-EM structure of human ABCG1 in complex with cholesterol and sphingomyelin
- Sphingomyelin is critical for ABCG1-mediated cholesterol efflux
- A cluster of Phe residues provide a hydrophobic exit to facilitate the substrate efflux
- Sequestration of cholesterol by acceptors is crucial for accomplishing the efflux cycle

Authors

Da Xu, Yanyan Li, Fengrui Yang, ..., Wen-Tao Hou, Cong-Zhao Zhou, Yuxing Chen

Correspondence

todvince@mail.ustc.edu.cn (W.-T.H.), zcz@ustc.edu.cn (C.-Z.Z.), cyxing@ustc.edu.cn (Y.C.)

In brief

The cryo-EM structure of human ABCG1 reported by Xu et al. reveals an ABCG1-driven cholesterol transport cycle initiated by sphingomyelin-assisted cholesterol recruitment and accomplished with cholesterol sequestration by the acceptors.

Xu et al., 2022, Cell Reports *38*, 110298
January 25, 2022
https://doi.org/10.1016/j.celrep.2022.110298

CellPress

Cell Reports

CellPress
OPEN ACCESS

Article

Structure and transport mechanism of the human cholesterol transporter ABCG1

Da Xu,[1] Yanyan Li,[2] Fengrui Yang,[3] Cai-Rong Sun,[1] Jinheng Pan,[2] Liang Wang,[1] Zhi-Peng Chen,[1] Shu-Cheng Fang,[1] Xuebiao Yao,[3] Wen-Tao Hou,[1,*] Cong-Zhao Zhou,[1,*] and Yuxing Chen[1,4,*]

[1]Division of Life Sciences and Medicine, University of Science and Technology of China, Hefei, Anhui 230027, China
[2]Key Laboratory of Structural Biology of Zhejiang Province, School of Life Sciences, Westlake University, Hangzhou, Zhejiang 310024, China
[3]MOE Key Laboratory for Cellular Dynamics, University of Science and Technology of China, Hefei, Anhui 230027, China
[4]Lead contact
*Correspondence: todvince@mail.ustc.edu.cn (W.-T.H.), zcz@ustc.edu.cn (C.-Z.Z.), cyxing@ustc.edu.cn (Y.C.)
https://doi.org/10.1016/j.celrep.2022.110298

SUMMARY

The reverse cholesterol transport pathway is responsible for the maintenance of human cholesterol homeostasis, an imbalance of which usually leads to atherosclerosis. As a key component of this pathway, the ATP-binding cassette transporter ABCG1 forwards cellular cholesterol to the extracellular acceptor nascent high-density lipoprotein (HDL). Here, we report a 3.26-Å cryo-electron microscopy structure of cholesterol-bound ABCG1 in an inward-facing conformation, which represents a turnover condition upon ATP binding. Structural analyses combined with functional assays reveals that a cluster of conserved hydrophobic residues, in addition to two sphingomyelins, constitute a well-defined cholesterol-binding cavity. The exit of this cavity is closed by three pairs of conserved Phe residues, which constitute a hydrophobic path for the release of cholesterol in an acceptor concentration-dependent manner. Overall, we propose an ABCG1-driven cholesterol transport cycle initiated by sphingomyelin-assisted cholesterol recruitment and accomplished by the release of cholesterol to HDL.

INTRODUCTION

As a major element of the plasma membrane of mammalian cells, cholesterol plays a pivotal role in multiple biological processes, such as maintaining the membrane fluidity and biosynthesis of bile acids, steroid hormones, and vitamin D (Schade et al., 2020). Cellular cholesterol homeostasis is subject to a finely tuned metabolic pathway. Dysfunction of this pathway will cause atherosclerosis (Luo et al., 2020; Schaftenaar et al., 2016) and in most cases eventually lead to the development of coronary atherosclerotic heart disease, which is currently the leading cause of death in the world. Beyond the *de novo* biosynthesis pathway, cholesterol can be taken up from extracellular sources via either low-density lipoprotein receptor from blood (Brown and Goldstein, 1986) or Niemann-Pick type C1-like 1 (NPC1L1) from the intestine and bile (Altmann et al., 2004). On the other hand, excess cellular cholesterol can be excreted from cells of peripheral tissues to the liver through the reverse cholesterol transport (RCT) pathway (Rosenson et al., 2012), which could prevent cholesterol-laden macrophages from being converted to foam cells, a hallmark of atherosclerotic disease (Bobryshev, 2006; Chistiakov et al., 2016; Stary et al., 1994; Wynn et al., 2013). As shown in Figure 1A, three ATP-binding cassette (ABC) transporters participate in cholesterol efflux in the RCT pathway (Luo et al., 2020). In macrophages, the excretion of cholesterol to the blood is first initiated by ABCA1, which transfers cellular cholesterol to lipid-free apolipoprotein A-I (apo A-I) to form discoidal nascent high-density lipoprotein (HDL) in the extracellular milieu (Favari et al., 2009; Tarling and Edwards, 2012; Vaughan and Oram, 2005). Afterward, ABCG1 pumps out more cellular cholesterol to the nascent HDL, and this process gradually drives the remodeling and maturation of HDL, which is eventually released to the plasma (Gelissen et al., 2006; Vaughan and Oram, 2006). In hepatocytes and enterocytes, excess cholesterol could be pumped out to the intestinal lumen and bile ducts by the heterodimeric ABC transporter ABCG5/8 (Graf et al., 2003; Wang et al., 2015). These transmembrane proteins are needed to guarantee intracellular cholesterol homeostasis for cellular and systemic functions (Luo et al., 2020).

The human *ABCG1* gene was first cloned in 1996 and identified as a homolog of the *white* gene in *Drosophila* (Chen et al., 1996; Savary et al., 1996). This gene was also sequentially termed *ABC8*, which encodes a regulator of cholesterol and phospholipid transport in macrophages (Klucken et al., 2000). A series of studies in mammalian cells as well as ABCG1-deficient mice have suggested that ABCG1 plays a critical role in the efflux of cellular cholesterol to HDL (Kennedy et al., 2005; Nakamura et al., 2004; Vaughan and Oram, 2005; Wang et al., 2004, 2006). As a key player in cholesterol efflux to HDL, *ABCG1* is also involved in tumor progression and the tumor immune response and has thus been proposed as a potential oncogene (Namba et al., 2018; Sag et al., 2015; Sharma and Agnihotri, 2019; Tian et al., 2017; Wang et al., 2016).

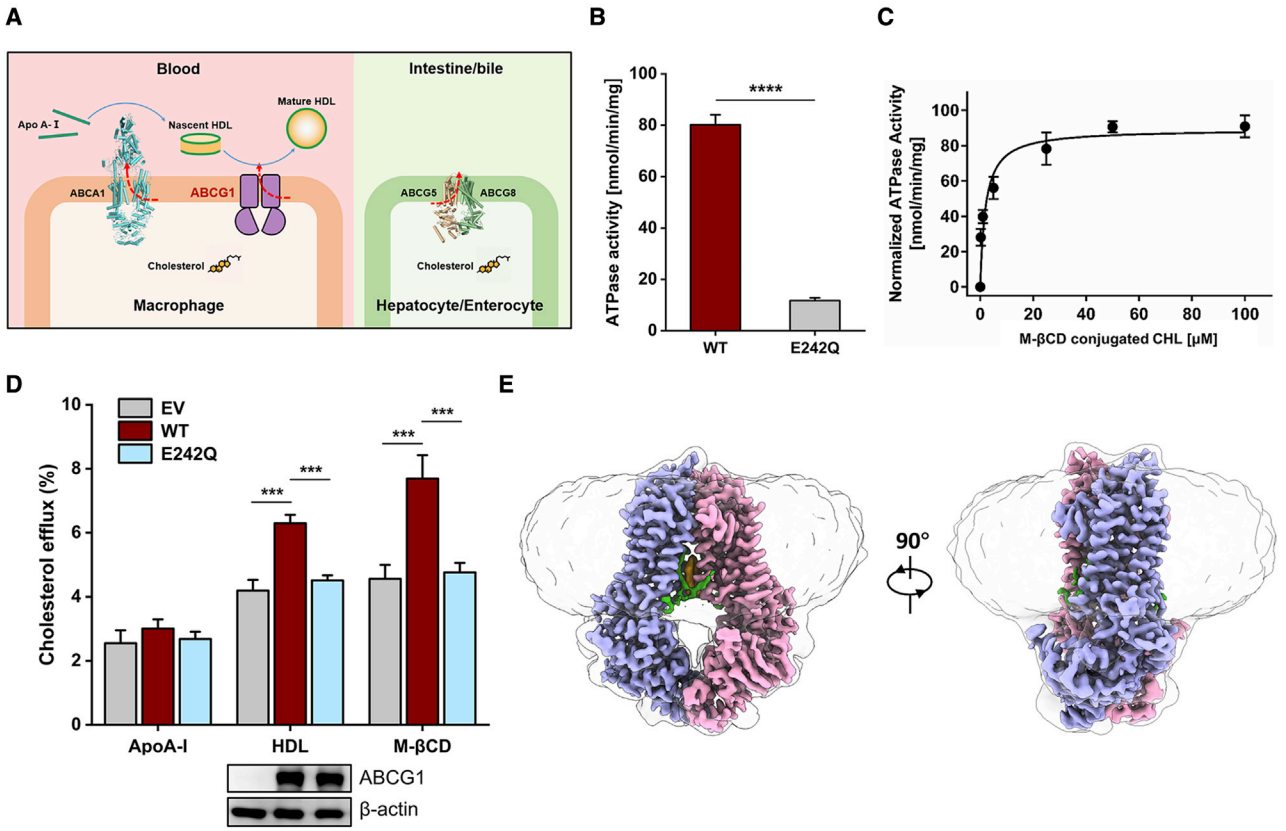

Figure 1. Function, activity assays, and structure determination of ABCG1

(A) A schematic diagram of ABC transporters involved in cholesterol translocation across the plasma membrane. The proteins of known structure include ABCA1 (PDB: 5XJY) and ABCG5/G8 (PDB: 5DO7). ABCG1, which is of unknown structure, is shown as a cartoon. ABCG1 and ABCA1 are expressed on the surface of macrophages, which are colored in cantaloupe, whereas ABCG5/ABCG8 heterodimers are expressed at the apical surface of enterocytes and hepatocytes, which are colored in pistachio. The directions of cholesterol translocation are indicated by dotted arrows.

(B) The ATPase activities of wild-type ABCG1 (WT) and E242Q mutant embedded in nanodiscs.

(C) Cholesterol-modulated ATPase activity of wild-type ABCG1 embedded in nanodiscs. The basal ATPase activity in the absence of cholesterol was normalized to zero. M-βCD and CHL are abbreviations for methyl-β-cyclodextrin and cholesterol, respectively.

(D) Cholesterol efflux assays with cells transfected with cDNA of wild-type ABCG1 (WT) and E242Q mutant. The empty vector (EV) was used as the negative control. The expression levels of the variants were quantified by western blot analysis of the total cell extracts, and β-actin served as an internal control. Each point represents the mean rate derived from at least three replicates. The standard deviations are indicated by error bars. Unpaired two-sided t test is used for the comparison of statistical significance in (B) and (D) The p values of <0.05, 0.01, 0.001, and 0.0001 are indicated with *, **, ***, and ****.

(E) Side views of 3D reconstruction of ABCG1-cholesterol complex. The two protomers of ABCG1 are colored in pink and purple, respectively. Four additional lipid-like densities in the cavity are colored in green and yellow, respectively. Densities of the detergent micelles are shown in gray.

See also Figures S1–S3 and S6 and Table S1.

The human ABCG subfamily consists of five members (ABCG1, ABCG2, ABCG4, ABCG5, and ABCG8), and all of these members are half-transporters that belong to the type V ABC transporters (Thomas and Tampé, 2020) and function in either homo or heterodimeric form. Notably, ABCG1 shares a sequence identity of 72% with ABCG4, which was previously suggested to function as a homodimer or a heterodimer with ABCG1 and might complement the function of ABCG1 (Cserepes et al., 2004; Hegyi and Homolya, 2016; Vaughan and Oram, 2006). In contrast, ABCG1 differs greatly from the other three members ABCG2/G5/G8 with a sequence identity of <30%. As the first high-resolution structure of the human ABCG transporter, the crystal structure of the heterodimer ABCG5/8 complex in the apo form was reported in 2016 (Lee et al., 2016). Afterward, a series of structures of ABCG2, a well-known multidrug transporter that effluxes anticancer drugs to the extracellular space (Allikmets et al., 1998; Doyle et al., 1998; Miyake et al., 1999), were solved by single-particle cryo-electron microscopy (cryo-EM) (Jackson et al., 2018; Khunweeraphong et al., 2017; Kowal et al., 2021; Manolaridis et al., 2018; Orlando and Liao, 2020; Taylor et al., 2017). However, the structure and transport mechanism of the rather distinct member ABCG1, which plays a central role in cholesterol homeostasis and protection against atherosclerosis, remains unknown.

Here, we report the cryo-EM structure of human ABCG1 in complex with cholesterol as a substrate at a resolution of 3.26 Å. Structural analysis combined with *in vitro* and cellular functional assays enabled us to identify the key residues for

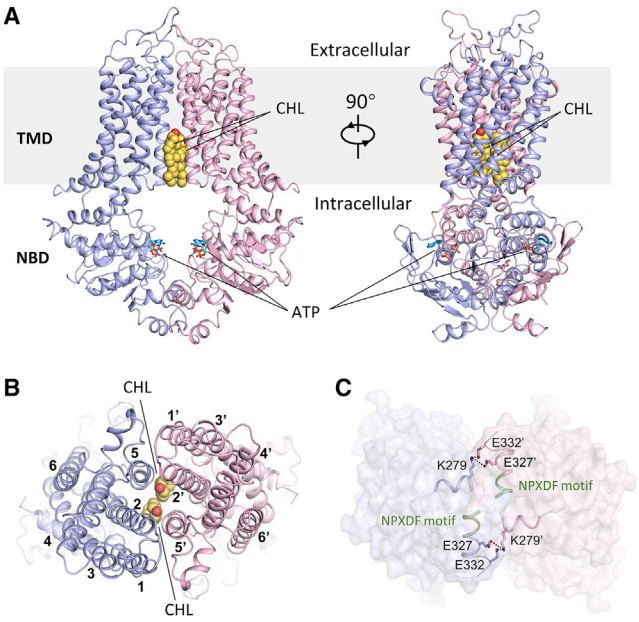

Figure 2. Overall structure of ABCG1

(A) The cartoon representation of ABCG1 in complex with cholesterol. The two protomers are colored in purple and pink, respectively. Two cholesterol molecules are shown in spheres, whereas two ATP molecules are shown in sticks. The membrane plane is indicated as the gray rectangle.

(B and C) View of ABCG1 from (B) the extracellular side or (C) the intracellular side. The six transmembrane helices of each protomer are labeled. The side chains of residues involved in the formation of salt bridges between two NBDs are shown in sticks, and the salt bridges are shown as dotted lines. The related segments are shown in a cartoon, and the NPXDF motifs are colored in green. See also Figure S4.

substrate binding and to uncover three pairs of Phe residues that are important for the release of substrate. In addition, we found two sphingomyelin molecules bound to the proximity of the substrate, which is necessary to assist the recruitment and alignment of cholesterol in the binding cavity. These findings not only advance our understanding of the molecular mechanism of cholesterol transport driven by ABCG1, but also provide hints for further therapeutic intervention in atherosclerosis.

RESULTS

Preparation and structural determination of ABCG1

Full-length human ABCG1, which is composed of 678 amino acid residues, was overexpressed in human embryonic kidney (HEK) 293F cells, extracted from the membrane fraction and purified with detergent for cryo-EM sample preparation. To mimic the physiological membrane environment, we reconstituted detergent-solubilized ABCG1 into lipid nanodiscs for biochemical assays. The purified ABCG1 in either detergent micelles or nanodiscs appeared to be stable and homogeneous, as confirmed by size-exclusion chromatography (Figures S1A and S1B). ABCG1 possesses a basal ATPase activity in the absence of cholesterol at 80.2 nmol ATP min^{-1} mg^{-1} protein, whereas the E242Q mutant, in which the catalytic residue Glu242 was replaced with glutamine, exhibited greatly decreased ATP hydrolysis activity (Figure 1B). Upon the addition of methyl-β-cyclodextrin (M-βCD)-conjugated cholesterol, ABCG1 embedded in nanodiscs (cholesterol free) showed an increased ATPase activity, yielding a half maximum effective concentration (EC_{50}) of 1.98 μM cholesterol and a V_{max} of 169.4 nmol ATP min^{-1} mg^{-1} protein (Figure 1C). Moreover, cellular cholesterol efflux assays indicated that the wild-type ABCG1 is capable of exporting intracellular cholesterol to HDL and M-βCD but not lipid-free apo A-I, and E242Q mutation led to a markedly reduced activity (Figure 1D). Notably, the recombinant FLAG-tagged ABCG1 proteins overexpressed in HEK 293T cells are localized on the ER and endosome (Figure S1C), despite the bona fide subcellular location of ABCG1 remaining controversial (Neufeld et al., 2014; Sano et al., 2014; Tarling and Edwards, 2011, 2016; Wang et al., 2006).

To obtain the structure of ABCG1 in the ATP-bound state, purified $ABCG1_{E242Q}$ in detergent micelles was incubated with 10 mM Mg^{2+}-ATP before cryo-EM sample preparation. Cryo-EM images of frozen hydrated samples revealed monodispersed ABCG1 homodimer particles (Figure S1D). After 2D and 3D classifications were performed with RELION3.1 (Scheres, 2012), 274,879 particles were selected and subtracted with a mask excluding the signal of detergent micelles and then imported into cryoSPARC3.2 (Punjani et al., 2017) for further classification and refinement (Figure S2A). Ultimately, 151,593 particles of the best class were refined with C2 symmetry, resulting in a 3.26-Å-resolution map according to the gold-standard Fourier shell correlation (FSC) 0.143 criterion (Figures S2B–S2D). The EM density exhibits prominent side-chain features in most segments (Figure S3), which allows us to unambiguously register the residues for all twelve transmembrane helices (TMs) and the core regions of nucleotide binding domains (NBDs). The final model of each protomer composed of residues Arg71–Arg675, with the exception of two flexible linker regions (Glu88-Lys95 and Gly334-Ser400), was refined against the EM density to obtain excellent geometry and statistics (Table S1). Unexpectedly, the structure revealed an inward-facing conformation in which the opposing Walker A and signature motifs are separated, even though two ATP molecules are bound to the NBDs (Figure S3). In addition, a group of branched lipid-like densities were observed in the transmembrane cavity and inner membrane interface, which indicated the copurification of endogenous lipids with recombinant ABCG1 (Figures 1E and S3).

Overall structure of ABCG1 in complex with cholesterol

Similar to other ABC half-transporters, two ABCG1 protomers formed a homodimer with two transmembrane domains (TMDs) and two NBDs, which bind and hydrolyze ATP for transporting the substrate across the membrane (Theodoulou and Kerr, 2015). The overall structure of ABCG1 adopts an inward-facing conformation, which involves the two TMDs folding without domain swapping (Figure 2A), a hallmark of the type V ABC transporter (Thomas and Tampé, 2020). Along the 2-fold axis, two TMDs form a cone-shaped transmembrane cavity surrounded by the TM2 and TM5 helices from each protomer that is open toward the cytoplasmic side and closed at the extracellular side (Figures 2A and 2B).

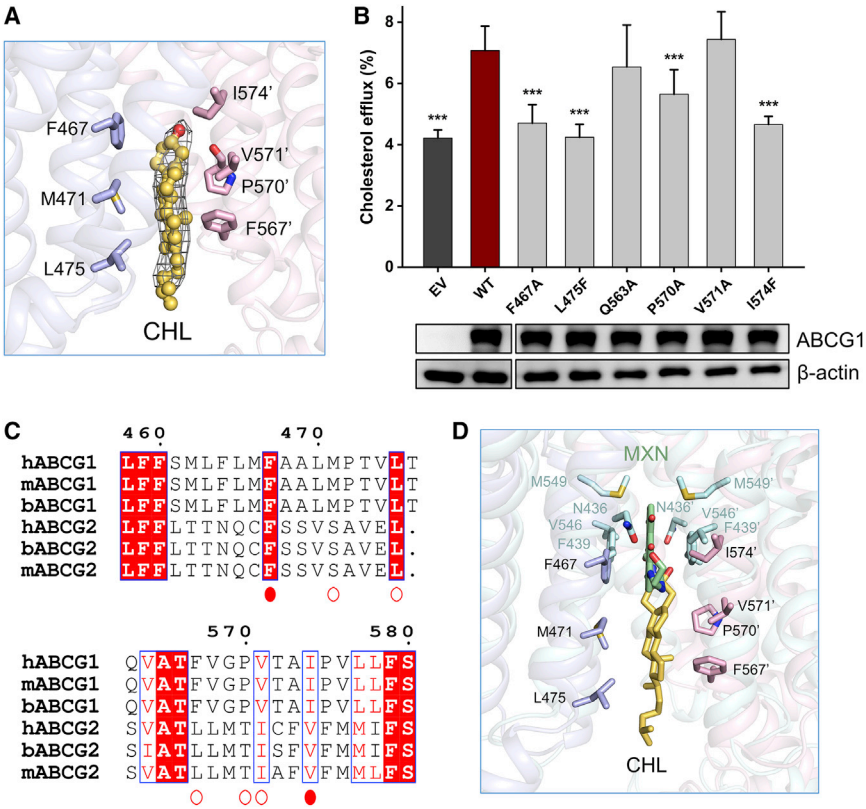

Figure 3. The interactions between ABCG1 and cholesterol

(A) The cholesterol-binding site. The cholesterol is shown in spheres and colored in yellow. Cholesterol-binding residues from each protomer are shown in sticks. The cholesterol is well fitted in the density (gray mesh), contoured at 5σ.

(B) The cholesterol efflux assays of ABCG1 with single mutations at the cholesterol-binding site. The assays were performed with cells transfected with cDNA of wild-type ABCG1 (WT) or corresponding mutants, with the empty vector (EV) as the negative control. The expression levels of the variants were quantified by western blot analysis of the total cell extracts, and β-actin served as an internal control. Each point represents the mean rate derived from at least four independent replicates. The standard deviations are indicated by error bars. Unpaired two-sided t test is used for the comparison of statistical significance. The p values of <0.05, 0.01, 0.001, and 0.0001 are indicated with *, **, ***, and ****, compared to the wild type.

(C) Sequence alignment of substrate-binding residues in ABCG1 and ABCG2. The sequences are from human (h), mouse (m), and bovine (b) ABCG1 or ABCG2. The substrate-binding residues in ABCG1 are marked by empty or solid circles. The two substrate-binding residues in ABCG1 and ABCG2 counterpart to each other are marked by solid circles.

(D) Structural superposition of the substrate-binding sites between ABCG1-cholesterol (purple/pink) and ABCG2-mitoxantrone (PDB: 6VXI, cyan). The side chains of substrate-binding residues are shown in sticks. CHL and MXN are abbreviations for cholesterol and mitoxantrone, respectively. CHL and MXN are shown in sticks and colored in yellow and green, respectively.

See also Figures S4 and S6.

The majority of the two NBDs are separated from each other, with a distance of ~22 Å between the Walker A motif and the opposing signature motif (Figure S4). In contrast, the distal moieties of NBDs are crosslinked via four pairs of salt bridges between Lys279 from one NBD and Glu327 and Glu322 from the other (Figure 2C). The two NBDs are also crosslinked in previously reported ABCG transporters via salt bridges from the conserved NPXDF motif (Jackson et al., 2018; Kowal et al., 2021; Manolaridis et al., 2018; Zhang et al., 2021). A previous cellular study found that mutations in the NPXDF motif of ABCG1 disrupt cholesterol efflux (Wang et al., 2013). However, our ABCG1 structure revealed that the NPXDF motif ($N^{320}PADF^{324}$) does not participate in the crosslinking of NBDs but provides a helical structure for the approaching of related residues. As shown in Figure 2A, two ATP molecules bind to the Walker A motifs of the separated NBDs, which indicates that the present structure of ABCG1 is under a turnover condition, a rather low-energy state during the transport cycle, as proposed in recent studies (Thaker et al., 2021; Yu et al., 2021).

We found two clear densities symmetrically located in the transmembrane cavity (Figure S3), and their contour is reminiscent of two polycyclic molecules. Accordingly, two putative polycyclic molecules, namely, cholesterol (CHL) and cholesteryl hemisuccinate (CHS), were fitted to the densities. In contrast to the steric clash upon CHS binding, a cholesterol molecule, as the substrate of ABCG1, perfectly matches the density (Figure S3). Notably, the two cholesterol molecules in our structure adopted a pose with the hydroxyl group pointing outwards, and this orientation is opposite to that in the plasma membrane. Similarly, cholesterol bound to ABCG2 also adopts this orientation (Taylor et al., 2017).

Two cholesterol molecules symmetrically bind to the TMDs

Two cholesterol molecules were aligned in parallel in the transmembrane cavity, with a distance of ~4 Å from each other (Figure 2B). Each cholesterol molecule forms extensive hydrophobic interactions with residues Phe467, Met471, and Leu475 from TM2 of one protomer and with Phe567, Pro570, Val571, and Ile574 from TM5 of the other protomer (Figure 3A). Site-directed mutagenesis-based cellular efflux activity assays indicated that these residues are important for cholesterol transport. Cells transfected with either the F467A or F567A mutant displayed significantly decreased cholesterol efflux activity (Figure 3B). The mutation of Leu475 or Ile574 to Phe fully disrupted the efflux activities compared with that of the wild type, which suggests that the aromatic side chain of Phe might induce a steric clash against cholesterol binding (Figure 3B). The mutation of Pro570, which engages a main-chain hydrogen bond with the hydroxyl group of cholesterol, led to a significant decrease in

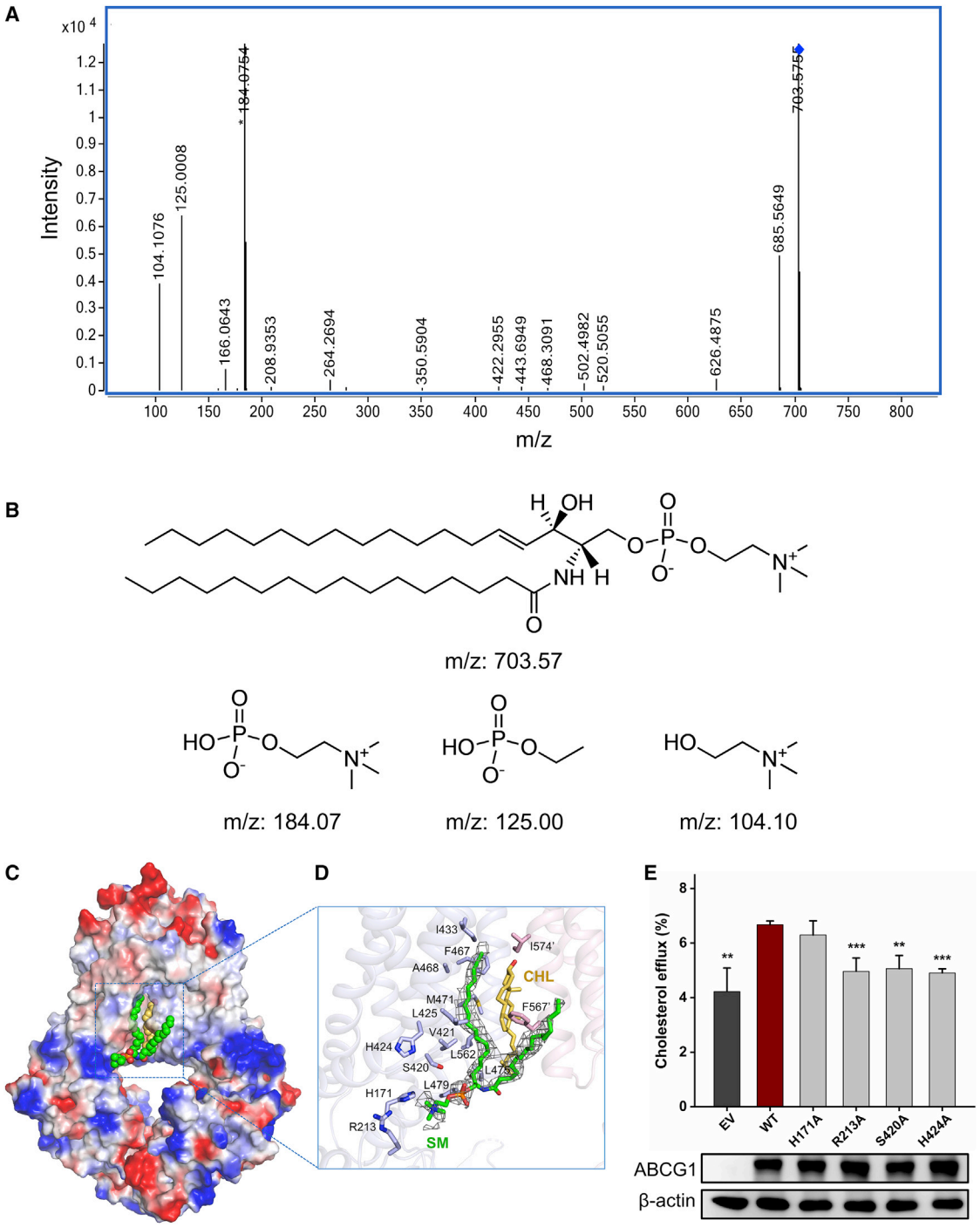

Figure 4. The sphingomyelin-binding site of ABCG1

(A) Tandem MS spectra of the fragments at *m/z* 703.57 from purified ABCG1 in detergent. The fragment at *m/z* 703.57 is consistent with sphingomyelin (d34:1).

(B) The potential MS/MS fragmentation pattern of sphingomyelin (d34:1).

(C) The sphingomyelin molecule binding to ABCG1. ABCG1 is color-coded by electrostatic potential ranging from blue (most positive) to red (most negative). Cholesterol and sphingomyelin molecules are shown in spheres and colored in yellow and green, respectively.

(D) The sphingomyelin-binding site. The residues surrounding sphingomyelin are shown in sticks. Cholesterol and sphingomyelin are shown in sticks and colored in yellow and green, respectively. The sphingomyelin molecule is well fitted to the density (gray mesh), contoured at 4σ.

(legend continued on next page)

cholesterol efflux activity. Multiple-sequence alignment revealed that these residues are conserved in ABCG1 orthologs (Figure 3C), which suggests that the hydrophobic environment is crucial for cholesterol transport. Notably, a hydrogen bond with the hydroxyl group of cholesterol has also been observed in other reported cholesterol-protein interaction patterns (Alam et al., 2019; Gimpl, 2016; Qian et al., 2020; Xu et al., 2021).

The overall structure of ABCG1 in complex with cholesterol is similar to the structures of anticancer drug-bound ABCG2 (Khunweeraphong et al., 2017; Manolaridis et al., 2018; Orlando and Liao, 2020). Taking ABCG2 in complex with mitoxantrone (MXN) as an example, an overall structural comparison revealed a root-mean-square deviation of 2.1 Å over 905 Cα atoms because ABCG1 exhibits a minor rigid body shift and rotation of TMD and NBD against that of ABCG2. However, ABCG1 exhibits marked differences from ABCG2 in terms of its substrate-binding pattern (Figures 3C and 3D). Two cholesterol molecules in ABCG1 are embedded in the inner membrane leaflet, whereas only one MXN molecule (Orlando and Liao, 2020) is observed in the deep transport cavity of ABCG2 (Figures 3D and S4B). Accordingly, only two substrate-binding residues (Phe439 and Val546) in ABCG2 can be superimposed against residues Phe467 and Ile574 in ABCG1 (Figure 3D), which are conserved between ABCG1 and ABCG2 (Figure 3C). In addition, the conserved π-π interactions provided by the pair of Phe439 from two TMDs of ABCG2, which is critical for aromatic substrate binding (Manolaridis et al., 2018; Orlando and Liao, 2020), are absent in ABCG1.

Two sphingomyelin molecules align in parallel with cholesterol

We found two additional densities showing a branched structure in the proximity of the two cholesterol molecules: one branch is oriented in parallel with the cholesterol chain, and the other branch extends to the membrane out of ABCG1 (Figure 1E). This structure is reminiscent of a phospholipid molecule, which is the major component of the plasma membrane. To identify the structure of this copurified molecule, we extracted lipids from the purified $ABCG1_{E242Q}$ sample in glycol-diosgenin (GDN) micelles and subjected these lipids to tandem mass spectrometry analysis. As predicted, sphingomyelin was detected and confirmed (Figures 4A, 4B, and S5 and Table S2). In fact, sphingomyelin has been previously identified as another substrate of ABCG1 beyond cholesterol (Kobayashi et al., 2006). Accordingly, we fit two sphingomyelin (d34:1) molecules into the branched densities (Figures 4C, 4D, and S3).

The polar head group of the sphingomyelin molecule is encompassed by a cluster of positively charged or polar residues, including His171 and Arg213 from the NBD and Ser420 and His424 from the TMD. One acyl chain of sphingomyelin is inserted into the detergent micelle, whereas the other acyl chain in parallel with cholesterol is stabilized by several lines of hydrophobic residues: Val421, Leu425, and Ile433 from TM1 of both protomers, Phe467, Ala468, Met471, Leu475, and Leu479 from TM2 of both protomers, Leu562 from TM5 of one protomer, and Phe567 and Ile574 from TM5 of the other protomer (Figure 4D). Moreover, this acyl chain of sphingomyelin forms extensive hydrophobic interactions with the α-face of cholesterol, which suggests that sphingomyelin should play a role in supporting the binding of cholesterol to ABCG1.

As previously reported, both ATPase and cholesterol efflux activities of ABCG1 could be stimulated in a sphingomyelin-dependent manner (Hirayama et al., 2013; Sano et al., 2007). We hence mutated the polar residues surrounding the phosphate group of sphingomyelin, including His171, Arg213, Ser420, and His424, to alanine. Activity assays revealed that cells transfected with the mutants R213A, S420A, and H424A but not H171A exhibited significantly decreased cholesterol efflux activities (Figure 4E). Moreover, the abundance ranking of SM in the lipids co-extracted from the mutants S420A, H424A, or S420A/H424A significantly decreased to seventh to about ninth, compared to the second to approximately third from the wild type or E242Q mutant (Table S2). Altogether, these data indicated that the presence of sphingomyelin is critical for ABCG1-mediated cholesterol efflux.

A Phe-rich exit from the transport cavity

In the present inward-facing structure of ABCG1, four pairs of Phe residues, namely, Phe459, Phe460, Phe582, and Phe583, from each protomer at the closed exit of the transport cavity form extensive intra- and inter-protomer hydrophobic interactions (Figure 5A). Multiple-sequence alignment indicated that Phe459 and Phe460 are highly conserved in all members of the ABCG subfamily, whereas Phe582 and Phe583 are conserved in ABCG1 transporters (Figure 5B). Cellular cholesterol efflux assays showed that the single mutation of Phe460, Phe582, or Phe583 to Ala resulted in a significant decrease in the transport activity, and an almost complete loss of activity was obtained with the F582A or F583A mutant (Figure 5C). In contrast, mutation of the somewhat distal Phe459 yielded an activity comparable to that of the wild type. Interestingly, the mutation of Leu554 in ABCG2 (corresponding to Phe582 of ABCG1) to Ala reportedly led to increased transport activity, which was proposed to serve as a "plug" during the transport cycle (Taylor et al., 2017). However, the mutation of F582L in ABCG1 showed no significant change in activity, whereas mutation of the succeeding Phe583 to Leu led to decreased efflux activity (Figure 5C), which suggested a different role of these Phe residues in ABCG1. The three pairs of Phe residues (Phe460, Phe582, and Phe583) in ABCG1 most likely provide a hydrophobic exit for substrate efflux.

(E) The cholesterol efflux assays of ABCG1 with single mutations at the sphingomyelin-binding site. The expression levels of the variants were quantified by western blot analysis of the total cell extracts, and β-actin served as an internal control. The assays were performed with cells transfected with cDNA of wild-type ABCG1 or mutants. Each point represents the mean rate derived from at least four independent replicates. The standard deviations are indicated by error bars. Unpaired two-sided t test is used for the comparison of statistical significance. The p values of <0.05, 0.01, 0.001, and 0.0001 are indicated with *, **, ***, and ****, compared to the wild type.
See also Figures S5 and S6 and Table S2.

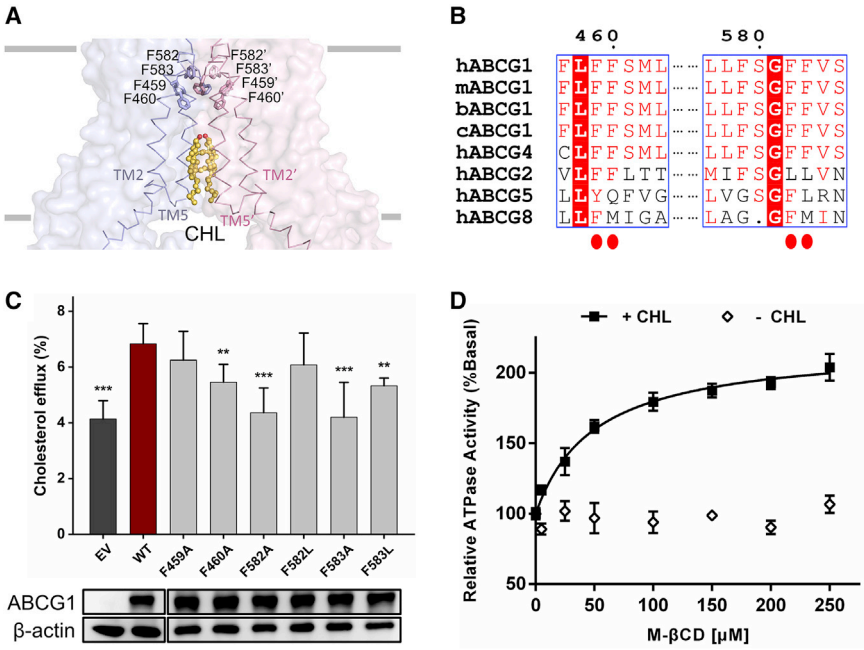

Figure 5. The Phe-rich exit of the transport cavity in ABCG1

(A) Four pairs of Phe residues at the exit of transport cavity of ABCG1. TM2 and TM5 helices are shown as ribbons, and Phe residues are shown in sticks.

(B) Sequence alignment of residues at the exit of the transport cavity in human ABCG subfamily transporters and other ABCG1 orthologs from mouse (m), bovine (b), and chicken (c). The four Phe residues are indicated by red solid circles.

(C) The cholesterol efflux assays of ABCG1 with single mutations at the Phe-rich exit. The expression levels of the variants were quantified by western blot analysis of the total cell extracts, and β-actin served as an internal control. The assays were performed with cells transfected with cDNA of wild-type ABCG1 (WT) or corresponding mutants, with the empty vector (EV) as the negative control. Each point represents the mean rate derived from at least four independent replicates. The standard deviations are indicated by error bars. Unpaired two-sided t test is used for the comparison of statistical significance. The p values of <0.05, 0.01, 0.001, and 0.0001 are indicated with *, **, ***, and ****, compared with the wild type.

(D) ATPase activities of ABCG1 embedded in nanodiscs upon the addition of M-βCD, in the presence (closed squares) or absence (open squares) of cholesterol. The basal ATPase activity in the presence and absence of cholesterol were both set to 100%. Data points analyzed above represent means of three independent measurements. The standard deviations are indicated by error bars.

See also Figure S6.

Cholesterol can be specifically presented via ABCG1 to acceptors such as nascent HDL *in vivo* or M-βCD *in vitro* rather than lipid-poor apo A-I, but not via free diffusion (Gelissen et al., 2006; Kennedy et al., 2005; Kobayashi et al., 2006; Vaughan and Oram, 2005; Wang et al., 2004). It is known that M-βCD could functionally mimic HDL to sequester cholesterol via hydrophobic interactions. We found that, in the presence of cholesterol, M-βCD could stimulate the ATPase activity of ABCG1 in a concentration-dependent manner (Figure 5D). It indicated that the sequestration of exported cholesterol by acceptors is crucial for accomplishing the full efflux cycle.

DISCUSSION

The RCT pathway is critical for the prevention of atherosclerosis and has thus been extensively investigated in the past half-century (Glomset et al., 1966; Ouimet et al., 2019; Rohatgi, 2019). However, the structure and transport mechanism of the key transporter ABCG1 that presents cellular cholesterol to nascent HDL remains unknown. Our present cryo-EM structure of the human cholesterol transporter ABCG1 in complex with cholesterol enables us to decipher more structural insights.

In the complex structure, two cholesterol molecules are captured in the transport cavity of TMDs via extensive hydrophobic interactions in addition to a couple of hydrogen bonds. Remarkably, two sphingomyelin molecules are bound to the TMDs, and one of the two acyl chains aligns in parallel with the cholesterol molecule, thus providing additional hydrophobic interactions to stabilize the cholesterol besides the two transmembrane helices TM2 and TM5. Moreover, the polar head group of sphingomyelin is surrounded by a couple of positively charged and polar residues. Site-directed mutagenesis combined with activity assays confirmed that these conserved residues are important for cholesterol efflux. These findings provide direct structural evidence supporting previous findings that sphingomyelin could stimulate the ATPase activity and cellular cholesterol efflux activity of ABCG1 (Hirayama et al., 2013; Sano et al., 2007). Moreover, cholesterols usually pack against sphingomyelin molecules to maintain the integrity and fluidity of the plasma membrane (Patzer and Wagner, 1978; Sezgin et al., 2017). It is plausible that the sphingomyelin molecule might also serve as a structural chaperone in combination with the transmembrane helices by forming a well-defined hydrophobic transport cavity for cholesterol. We hence speculated that the sphingomyelin molecule should assist the recruitment and proper orientation of cholesterol and thus directly participates in initiating substrate transport.

In addition, cholesterol molecules are sealed in the transport cavity via three pairs of Phe residues at the exit in our present inward-facing structure. Mutagenesis combined with cellular cholesterol efflux assays revealed that these Phe residues are indispensable for ABCG1 transport activity. Given the hydrophobic property of Phe residues, these residues not only constitute a hydrophobic path for the release of cholesterol but also provide a gating mechanism to avoid the release of substrates in the absence of extracellular cholesterol acceptors.

Based on our ABCG1-cholesterol-ATP structure and biochemical analysis of ABCG1, combined with the recent reports during the revision of this manuscript (Skarda et al., 2021; Sun et al., 2021), we proposed a putative transport cycle

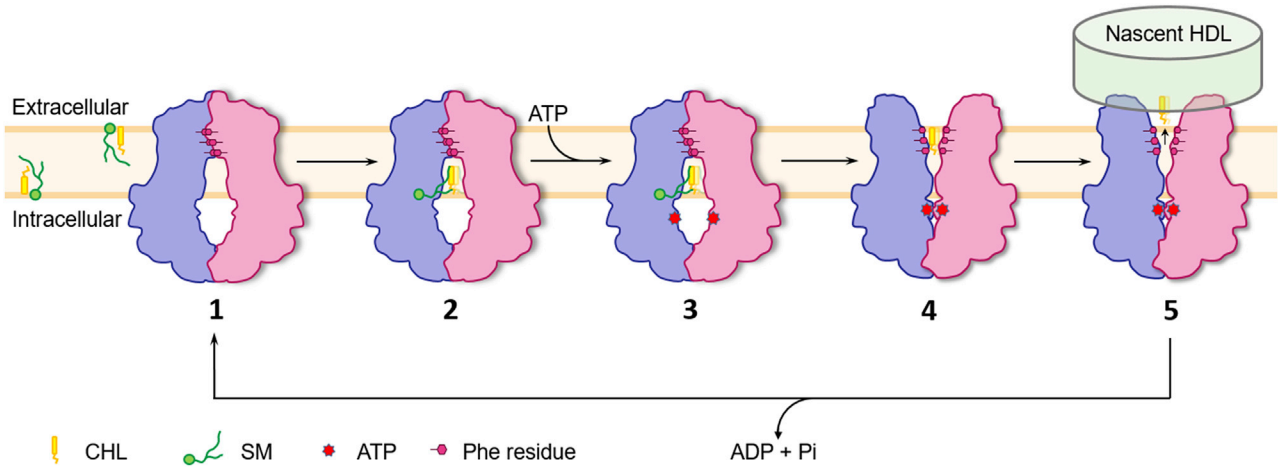

Figure 6. A proposed cycle of cholesterol transport driven by ABCG1

The transport cycle consists of five conformational states: the rest state of the apo form (State 1), the inward-facing conformation with simultaneous binding of cholesterol and sphingomyelin (State 2), the turnover state upon ATP binding (State 3), the outward-facing conformation with cholesterol passing the Phe-rich exit (State 4), and the last, the cholesterol release to the acceptor (State 5). The two ABCG1 protomers are colored in purple and pink, respectively.

model of ABCG1 (Figure 6). Initially, the apo-form ABCG1 adopts an inward-facing conformation (State 1). Due to free diffusion in the plasma membrane, sphingomyelin and cholesterol molecules simultaneously bind to ABCG1, which results in the formation of an intact hydrophobic transport cavity together with the helices TM2 and TM5 (State 2). Upon the binding of ATP to the NBDs, ABCG1 adopts a turnover condition from the inward-facing state, which was captured in our structure (State 3), to the highly transient outward-facing state (State 4). Consequently, the Phe-rich exit opens toward the extracellular space, but this hydrophobic exit retains cholesterol molecules in the absence of extracellular acceptors. Once nascent HDL attaches to ABCG1 from the extracellular side, cholesterol molecules are engulfed from the Phe-rich exit to HDL (State 5), which mimics a very hydrophobic sponge. Subsequently, accompanied by ATP hydrolysis and the release of cholesterol molecules, the Phe-rich exit recloses, and ABCG1 is reset to the rest state (State 1).

Limitations of the study

We determined the structure of ABCG1 in complex with cholesterol and ATP molecules, and also revealed the importance of the sphingomyelin molecules binding in the substrate cavity for cholesterol efflux. Although previous studies revealed that ABCG1 could mediate the efflux of sphingomyelin, whether sphingomyelin is co-effluxed with cholesterol remains unclear. Further investigations are needed to illustrate how sphingomyelin participates in the ABCG1-driven cholesterol translocation.

STAR★METHODS

Detailed methods are provided in the online version of this paper and include the following:

- KEY RESOURCES TABLE
- RESOURCE AVAILABILITY
  - Lead contact
  - Materials availability
  - Data and code availability
- EXPERIMENTAL MODEL AND SUBJECT DETAILS
  - Cell culture
- METHOD DETAILS
  - Protein expression and purification
  - Nanodiscs preparation
  - ATPase activity assay
  - Lipid purification and mass spectrometry
  - Cellular cholesterol efflux assay
  - Western blot analysis
  - Cryo-EM sample preparation and data collection
  - Image processing
  - Model building and refinement
  - Immunofluorescence
  - Microscale fluorescent thermal stability assay
- QUANTIFICATION AND STATISTICAL ANALYSIS

SUPPLEMENTAL INFORMATION

Supplemental information can be found online at https://doi.org/10.1016/j.celrep.2022.110298.

ACKNOWLEDGMENTS

We thank Yongxiang Gao and Zhenyu Qiu at the Center for Integrative Imaging, Hefei National Laboratory for Physical Sciences at the Microscale, University of Science and Technology of China, for technical supports during cryo-EM image acquisition. We thank Jishu Ren at the Isotope Laboratory, University of Science and Technology of China, for the transport assays. This work is supported by the Ministry of Science and Technology of the People's Republic of China (2020YFA0509302), the Fundamental Research Funds for the Central Universities (YD9100002014), the Strategic Priority Research Program of the Chinese Academy of Sciences (XDB37020202), and the National Natural Science Foundation of China grants 91854203.

AUTHOR CONTRIBUTIONS

D.X. and Y.C. conceptualized this study. C.-Z.Z. and Y.C. supervised the project. D.X. and W.-T.H. designed all the experiments. D.X. performed cloning, expression, purification, EM sample preparation, screening, and analyses of human ABCG1. D.X. and C.-R.S. preformed cryo-EM data collection. D.X. and Z.-P.C. performed ATPase activity assays. D.X. and W.-T.H. performed cholesterol efflux assays. Y.L. and J.P. performed mass spectrometry analyses. D.X. and L.W. performed structure determination and model refinement. F.Y. performed cell imaging. All authors contributed to data analysis. D.X., W.-T.H., C.-Z.Z., and Y.C. wrote the manuscript.

DECLARATION OF INTERESTS

The authors declare no competing interests.

Received: July 20, 2021
Revised: December 13, 2021
Accepted: January 4, 2022
Published: January 25, 2022

REFERENCES

Adams, P.D., Afonine, P.V., Bunkóczi, G., Chen, V.B., Davis, I.W., Echols, N., Headd, J.J., Hung, L.W., Kapral, G.J., Grosse-Kunstleve, R.W., et al. (2010). PHENIX: a comprehensive Python-based system for macromolecular structure solution. Acta Crystallogr. D Biol. Crystallogr. *66*, 213–221.

Alam, A., Kowal, J., Broude, E., Roninson, I., and Locher, K.P. (2019). Structural insight into substrate and inhibitor discrimination by human P-glycoprotein. Science *363*, 753–756.

Alexandrov, A.I., Mileni, M., Chien, E.Y., Hanson, M.A., and Stevens, R.C. (2008). Microscale fluorescent thermal stability assay for membrane proteins. Structure *16*, 351–359.

Allikmets, R., Schriml, L.M., Hutchinson, A., Romano-Spica, V., and Dean, M. (1998). A human placenta-specific ATP-binding cassette gene (*ABCP*) on chromosome 4q22 that is involved in multidrug resistance. Cancer Res. *58*, 5337.

Altmann, S.W., Davis, H.R., Zhu, L.-j., Yao, X., Hoos, L.M., Tetzloff, G., Iyer, S.P.N., Maguire, M., Golovko, A., Zeng, M., et al. (2004). Niemann-pick C1 like 1 protein is critical for intestinal cholesterol absorption. Science *303*, 1201.

Bobryshev, Y.V. (2006). Monocyte recruitment and foam cell formation in atherosclerosis. Micron *37*, 208–222.

Brown, M.S., and Goldstein, J.L. (1986). A receptor-mediated pathway for cholesterol homeostasis. Science *232*, 34.

Chen, H., Rossier, C., Lalioti, M.D., Lynn, A., Chakravarti, A., Perrin, G., and Antonarakis, S.E. (1996). Cloning of the cDNA for a human homologue of the *Drosophila white* gene and mapping to chromosome 21q22.3. Am. J. Hum. Genet. *59*, 66–75.

Chen, V.B., Arendall, W.B., Headd, J.J., Keedy, D.A., Immormino, R.M., Kapral, G.J., Murray, L.W., Richardson, J.S., and Richardson, D.C. (2010). MolProbity: all-atom structure validation for macromolecular crystallography. Acta Crystallogr. D, Biol. Crystallogr. *66*, 12–21.

Chistiakov, D.A., Bobryshev, Y.V., and Orekhov, A.N. (2016). Macrophage-mediated cholesterol handling in atherosclerosis. J. Cell Mol. Med. *20*, 17–28.

Corpet, F. (1988). Multiple sequence alignment with hierarchical clustering. Nucleic Acids Res. *16*, 10881–10890.

Cserepes, J., Szentpétery, Z., Seres, L., Özvegy-Laczka, C., Langmann, T., Schmitz, G., Glavinas, H., Klein, I., Homolya, L., Váradi, A., et al. (2004). Functional expression and characterization of the human ABCG1 and ABCG4 proteins: indications for heterodimerization. Biochem. Biophys. Res. Commun. *320*, 860–867.

Davis, I.W., Leaver-Fay, A., Chen, V.B., Block, J.N., Kapral, G.J., Wang, X., Murray, L.W., Arendall, W.B., Snoeyink, J., Richardson, J.S., et al. (2007). MolProbity: all-atom contacts and structure validation for proteins and nucleic acids. Nucleic Acids Res. *35*, W375–W383.

Doyle, L.A., Yang, W., Abruzzo, L.V., Krogmann, T., Gao, Y., Rishi, A.K., and Ross, D.D. (1998). A multidrug resistance transporter from human MCF-7 breast cancer cells. Proc. Natl. Acad. Sci. *95*, 15665.

Emsley, P., and Cowtan, K. (2004). Coot: model-building tools for molecular graphics. Acta Crystallogr. D Biol. Crystallogr. *60*, 2126–2132.

Emsley, P., Lohkamp, B., Scott, W.G., and Cowtan, K. (2010). Features and development of Coot. Acta Crystallogr. D Biol. Crystallogr. *66*, 486–501.

Favari, E., Calabresi, L., Adorni, M.P., Jessup, W., Simonelli, S., Franceschini, G., and Bernini, F. (2009). Small discoidal pre-β1 HDL particles are efficient acceptors of cell cholesterol via ABCA1 and ABCG1. Biochemistry *48*, 11067–11074.

Gelissen, I.C., Harris, M., Rye, K.-A., Quinn, C., Brown, A.J., Kockx, M., Cartland, S., Packianathan, M., Kritharides, L., and Jessup, W. (2006). ABCA1 and ABCG1 synergize to mediate cholesterol export to ApoA-I. Arterioscler. Thromb. Vasc. Biol. *26*, 534–540.

Gimpl, G. (2016). Interaction of G protein coupled receptors and cholesterol. Chem. Phys. Lipids *199*, 61–73.

Glomset, J.A., Janssen, E.T., Kennedy, R., and Dobbins, J. (1966). Role of plasma lecithin:cholesterol acyltransferase in the metabolism of high density lipoproteins. J. Lipid Res. *7*, 638–648.

Graf, G.A., Yu, L., Li, W.-P., Gerard, R., Tuma, P.L., Cohen, J.C., and Hobbs, H.H. (2003). ABCG5 and ABCG8 are obligate heterodimers for protein trafficking and biliary cholesterol excretion. J. Biol. Chem. *278*, 48275–48282.

Hegyi, Z., and Homolya, L. (2016). Functional cooperativity between ABCG4 and ABCG1 isoforms. PLoS One *11*, e0156516.

Hirayama, H., Kimura, Y., Kioka, N., Matsuo, M., and Ueda, K. (2013). ATPase activity of human ABCG1 is stimulated by cholesterol and sphingomyelin. J. Lipid Res. *54*, 496–502.

Jackson, S.M., Manolaridis, I., Kowal, J., Zechner, M., Taylor, N.M.I., Bause, M., Bauer, S., Bartholomaeus, R., Bernhardt, G., Koenig, B., et al. (2018). Structural basis of small-molecule inhibition of human multidrug transporter ABCG2. Nat. Struct. Mol. Biol. *25*, 333–340.

Kennedy, M.A., Barrera, G.C., Nakamura, K., Baldán, Á., Tarr, P., Fishbein, M.C., Frank, J., Francone, O.L., and Edwards, P.A. (2005). ABCG1 has a critical role in mediating cholesterol efflux to HDL and preventing cellular lipid accumulation. Cell Metab. *1*, 121–131.

Khunweeraphong, N., Stockner, T., and Kuchler, K. (2017). The structure of the human ABC transporter ABCG2 reveals a novel mechanism for drug extrusion. Scientific Rep. *7*, 13767.

Klucken, J., Büchler, C., Orsó, E., Kaminski, W.E., Porsch-Özcürümez, M., Liebisch, G., Kapinsky, M., Diederich, W., Drobnik, W., Dean, M., et al. (2000). ABCG1 (ABC8), the human homolog of the *Drosophila white* gene, is a regulator of macrophage cholesterol and phospholipid transport. Proc. Natl. Acad. Sci. *97*, 817.

Kobayashi, A., Takanezawa, Y., Hirata, T., Shimizu, Y., Misasa, K., Kioka, N., Arai, H., Ueda, K., and Matsuo, M. (2006). Efflux of sphingomyelin, cholesterol, and phosphatidylcholine by ABCG1. J. Lipid Res. *47*, 1791–1802.

Kowal, J., Ni, D., Jackson, S.M., Manolaridis, I., Stahlberg, H., and Locher, K.P. (2021). Structural basis of drug recognition by the multidrug transporter ABCG2. J. Mol. Biol. *433*, 166980.

Kucukelbir, A., Sigworth, F.J., and Tagare, H.D. (2014). Quantifying the local resolution of cryo-EM density maps. Nat. Methods *11*, 63–65.

Lee, J.-Y., Kinch, L.N., Borek, D.M., Wang, J., Wang, J., Urbatsch, I.L., Xie, X.-S., Grishin, N.V., Cohen, J.C., Otwinowski, Z., et al. (2016). Crystal structure of the human sterol transporter ABCG5/ABCG8. Nature *533*, 561–564.

Luo, J., Yang, H., and Song, B.-L. (2020). Mechanisms and regulation of cholesterol homeostasis. Nat. Rev. Mol. Cell Biol. *21*, 225–245.

Manolaridis, I., Jackson, S.M., Taylor, N.M.I., Kowal, J., Stahlberg, H., and Locher, K.P. (2018). Cryo-EM structures of a human ABCG2 mutant trapped in ATP-bound and substrate-bound states. Nature *563*, 426–430.

Mastronarde, D.N. (2005). Automated electron microscope tomography using robust prediction of specimen movements. J. Struct. Biol. *152*, 36–51.

Miyake, K., Mickley, L., Litman, T., Zhan, Z., Robey, R., Cristensen, B., Brangi, M., Greenberger, L., Dean, M., Fojo, T., et al. (1999). Molecular cloning of cDNAs which are highly overexpressed in mitoxantrone-resistant cells. Cancer Res. *59*, 8.

Nakamura, K., Kennedy, M.A., Baldán, Á., Bojanic, D.D., Lyons, K., and Edwards, P.A. (2004). Expression and regulation of multiple murine ATP-binding cassette transporter G1 mRNAs/isoforms that stimulate cellular cholesterol efflux to high density lipoprotein. J. Biol. Chem. *279*, 45980–45989.

Namba, Y., Sogawa, C., Okusha, Y., Kawai, H., Itagaki, M., Ono, K., Murakami, J., Aoyama, E., Ohyama, K., Asaumi, J.-i., et al. (2018). Depletion of lipid efflux pump ABCG1 triggers the intracellular accumulation of extracellular vesicles and reduces aggregation and tumorigenesis of metastatic cancer cells. Front. Oncol. *8*, 376.

Neufeld, E.B., O'Brien, K., Walts, A.D., Stonik, J.A., Demosky, S.J., Malide, D., Combs, C.A., and Remaley, A.T. (2014). Cellular localization and trafficking of the human ABCG1 transporter. Biology *3*, 781–800.

Orlando, B.J., and Liao, M. (2020). ABCG2 transports anticancer drugs via a closed-to-open switch. Nat. Commun. *11*, 2264.

Ouimet, M., Barrett, T.J., and Fisher, E.A. (2019). HDL and reverse cholesterol transport. Circ. Res. *124*, 1505–1518.

Patzer, E.J., and Wagner, R.R. (1978). Cholesterol oxidase as a probe for studying membrane organisation. Nature *274*, 394–395.

Pettersen, E.F., Goddard, T.D., Huang, C.C., Couch, G.S., Greenblatt, D.M., Meng, E.C., and Ferrin, T.E. (2004). UCSF Chimera–a visualization system for exploratory research and analysis. J. Comput. Chem. *25*, 1605–1612.

Pettersen, E.F., Goddard, T.D., Huang, C.C., Meng, E.C., Couch, G.S., Croll, T.I., Morris, J.H., and Ferrin, T.E. (2021). UCSF ChimeraX: structure visualization for researchers, educators, and developers. Protein Sci. *30*, 70–82.

Punjani, A., Rubinstein, J.L., Fleet, D.J., and Brubaker, M.A. (2017). cryoSPARC: algorithms for rapid unsupervised cryo-EM structure determination. Nat. Methods *14*, 290–296.

Qian, H., Wu, X., Du, X., Yao, X., Zhao, X., Lee, J., Yang, H., and Yan, N. (2020). Structural basis of low-pH-dependent lysosomal cholesterol egress by NPC1 and NPC2. Cell *182*, 98–111.e8.

Rohatgi, A. (2019). Reverse cholesterol transport and atherosclerosis. Arterioscler. Thromb. Vasc. Biol. *39*, 2–4.

Rohou, A., and Grigorieff, N. (2015). CTFFIND4: fast and accurate defocus estimation from electron micrographs. J. Struct. Biol. *192*, 216–221.

Rosenson, R.S., Brewer, H.B., Davidson, W.S., Fayad, Z.A., Fuster, V., Goldstein, J., Hellerstein, M., Jiang, X.-C., Phillips, M.C., Rader, D.J., et al. (2012). Cholesterol efflux and atheroprotection. Circulation *125*, 1905–1919.

Rosenthal, P.B., and Henderson, R. (2003). Optimal determination of particle orientation, absolute hand, and contrast loss in single-particle electron cryomicroscopy. J. Mol. Biol. *333*, 721–745.

Sag, D., Cekic, C., Wu, R., Linden, J., and Hedrick, C.C. (2015). The cholesterol transporter ABCG1 links cholesterol homeostasis and tumour immunity. Nat. Commun. *6*, 6354.

Sano, O., Ito, S., Kato, R., Shimizu, Y., Kobayashi, A., Kimura, Y., Kioka, N., Hanada, K., Ueda, K., and Matsuo, M. (2014). ABCA1, ABCG1, and ABCG4 are distributed to distinct membrane meso-domains and disturb detergent-resistant domains on the plasma membrane. PLoS One *9*, e109886.

Sano, O., Kobayashi, A., Nagao, K., Kumagai, K., Kioka, N., Hanada, K., Ueda, K., and Matsuo, M. (2007). Sphingomyelin-dependence of cholesterol efflux mediated by ABCG1. J. Lipid Res. *48*, 2377–2384.

Savary, S., Denizot, F., Luciani, M.F., Mattei, M.G., and Chimini, G. (1996). Molecular cloning of a mammalian ABC transporter homologous to Drosophila white gene. Mamm. Genome *7*, 673–676.

Schade, D.S., Shey, L., and Eaton, R.P. (2020). Cholesterol review: a metabolically important molecule. Endocr. Pract. *26*, 1514–1523.

Schaftenaar, F., Frodermann, V., Kuiper, J., and Lutgens, E. (2016). Atherosclerosis: the interplay between lipids and immune cells. Curr. Opin. Lipidol. *27*, 209–215.

Scheres, S.H. (2012). RELION: implementation of a Bayesian approach to cryo-EM structure determination. J. Struct. Biol. *180*, 519–530.

Schneider, C.A., Rasband, W.S., and Eliceiri, K.W. (2012). NIH Image to ImageJ: 25 years of image analysis. Nat. Methods *9*, 671–675.

Sezgin, E., Levental, I., Mayor, S., and Eggeling, C. (2017). The mystery of membrane organization: composition, regulation and roles of lipid rafts. Nat. Rev. Mol. Cell Biol. *18*, 361–374.

Sharma, B., and Agnihotri, N. (2019). Role of cholesterol homeostasis and its efflux pathways in cancer progression. J. Steroid Biochem. Mol. Biol. *191*, 105377.

Skarda, L., Kowal, J., and Locher, K.P. (2021). Structure of the human cholesterol transporter ABCG1. J. Mol. Biol. *433*, 167218.

Stary, H.C., Chandler, A.B., Glagov, S., Guyton, J.R., Insull, W., Rosenfeld, M.E., Schaffer, S.A., Schwartz, C.J., Wagner, W.D., and Wissler, R.W. (1994). A definition of initial, fatty streak, and intermediate lesions of atherosclerosis. A report from the Committee on Vascular Lesions of the Council on Arteriosclerosis, American Heart Association. Circulation *89*, 2462–2478.

Sun, Y., Wang, J., Long, T., Qi, X., Donnelly, L., Elghobashi-Meinhardt, N., Esparza, L., Cohen, J.C., Xie, X.S., Hobbs, H.H., et al. (2021). Molecular basis of cholesterol efflux via ABCG subfamily transporters. Proc. Natl. Acad. Sci. U S A. *118*, e2110483118.

Tarling, E.J., and Edwards, P.A. (2011). ATP binding cassette transporter G1 (ABCG1) is an intracellular sterol transporter. Proc. Natl. Acad. Sci. U S A. *108*, 19719.

Tarling, E.J., and Edwards, P.A. (2012). Dancing with the sterols: critical roles for ABCG1, ABCA1, miRNAs, and nuclear and cell surface receptors in controlling cellular sterol homeostasis. Biochim. Biophys. Acta Mol. Cell Biol. Lipids *1821*, 386–395.

Tarling, E.J., and Edwards, P.A. (2016). Intracellular localization of endogenous mouse ABCG1 is mimicked by both ABCG1-I550 and ABCG1-P550-brief report. Arterioscler Thromb. Vasc. Biol. *36*, 1323–1327.

Taylor, N.M.I., Manolaridis, I., Jackson, S.M., Kowal, J., Stahlberg, H., and Locher, K.P. (2017). Structure of the human multidrug transporter ABCG2. Nature *546*, 504–509.

Thaker, T.M., Mishra, S., Zhou, W., Faraldo-Gomez, J.D., McHaourab, H.S., and Tomasiak, T.M. (2021). Cryo-EM structure of an elusive pre-transport intermediate of the multidrug ABC transporter BmrCD reveals modes of asymmetric drug binding. bioRxiv, 2021.2003.2013.435271.

Theodoulou, Frederica L., and Kerr, Ian D. (2015). ABC transporter research: going strong 40 years on. Biochem. Soc. Trans. *43*, 1033–1040.

Thomas, C., and Tampé, R. (2020). Structural and mechanistic principles of ABC transporters. Annu. Rev. Biochem. *89*, 605–636.

Tian, C., Huang, D., Yu, Y., Zhang, J., Fang, Q., and Xie, C. (2017). ABCG1 as a potential oncogene in lung cancer. Exp. Ther. Med. *13*, 3189–3194.

Vaughan, A.M., and Oram, J.F. (2005). ABCG1 redistributes cell cholesterol to domains removable by high density lipoprotein but not by lipid-depleted apolipoproteins. J. Biol. Chem. *280*, 30150–30157.

Vaughan, A.M., and Oram, J.F. (2006). ABCA1 and ABCG1 or ABCG4 act sequentially to remove cellular cholesterol and generate cholesterol-rich HDL. J. Lipid Res. *47*, 2433–2443.

Wang, F., Li, G., Gu, H.M., and Zhang, D.W. (2013). Characterization of the role of a highly conserved sequence in ATP binding cassette transporter G (ABCG) family in ABCG1 stability, oligomerization, and trafficking. Biochemistry *52*, 9497–9509.

Wang, J., Mitsche, M.A., Lütjohann, D., Cohen, J.C., Xie, X.-S., and Hobbs, H.H. (2015). Relative roles of ABCG5/ABCG8 in liver and intestine. J. Lipid Res. *56*, 319–330.

Wang, N., Lan, D., Chen, W., Matsuura, F., and Tall, A.R. (2004). ATP-binding cassette transporters G1 and G4 mediate cellular cholesterol efflux to high-density lipoproteins. Proc. Natl. Acad. Sci. U S A. *101*, 9774.

Wang, N., Ranalletta, M., Matsuura, F., Peng, F., and Tall Alan, R. (2006). LXR-induced redistribution of ABCG1 to plasma membrane in macrophages enhances cholesterol mass efflux to HDL. Arterioscler. Thromb. Vasc. Biol. *26*, 1310–1316.

Wang, Y., Liu, H., Ready, N.E., Su, L., Wei, Y., Christiani, D.C., and Wei, Q. (2016). Genetic variants in ABCG1 are associated with survival of nonsmall-cell lung cancer patients. Int. J. Cancer *138*, 2592–2601.

Wynn, T.A., Chawla, A., and Pollard, J.W. (2013). Macrophage biology in development, homeostasis and disease. Nature *496*, 445–455.

Xu, P., Huang, S., Zhang, H., Mao, C., Zhou, X.E., Cheng, X., Simon, I.A., Shen, D.D., Yen, H.Y., Robinson, C.V., et al. (2021). Structural insights into the lipid and ligand regulation of serotonin receptors. Nature *592*, 469–473.

Yu, Q., Ni, D., Kowal, J., Manolaridis, I., Jackson, S.M., Stahlberg, H., and Locher, K.P. (2021). Structures of ABCG2 under turnover conditions reveal a key step in the drug transport mechanism. Nat. Commun. *12*, 4376.

Zhang, H., Huang, C.-S., Yu, X., Lee, J., Vaish, A., Chen, Q., Zhou, M., Wang, Z., and Min, X. (2021). Cryo-EM structure of ABCG5/G8 in complex with modulating antibodies. Commun. Biol. *4*, 526.

Zheng, S.Q., Palovcak, E., Armache, J.P., Verba, K.A., Cheng, Y., and Agard, D.A. (2017). MotionCor2: anisotropic correction of beam-induced motion for improved cryo-electron microscopy. Nature Methods, 331–332. https://doi.org/10.1038/nmeth.4193.

STAR★METHODS

KEY RESOURCES TABLE

REAGENT or RESOURCE	SOURCE	IDENTIFIER
Antibodies		
Mouse monoclonal anti-FLAG	Proteintech	Cat#66008-3-Ig
Mouse monoclonal anti-β-actin	Proteintech	Cat#66009-1-Ig; RRID:AB_2687938
HRP-conjugated goat anti-Mouse IgG(H+L)	Proteintech	Cat#SA00001-1; RRID:AB_2722565
Rabbit polyclonal anti-FLAG	Sigma Aldrich	Cat#F7425; RRID:AB_439687
Goat anti-Rabbit FITC	Jackson ImmunoResearch	Cat#111-095-003; RRID:AB_2337972
Bacterial and virus strains		
TOP10 Chemically Competent Cells	Tsingke Biological Technology	Cat#TSC-C12
Chemicals, peptides, and recombinant proteins		
SMM 293-TII Expression Medium	Sino Biological	Cat#M293TII
Polyethylenimine, Linear, MW 25000	Polysciences	Cat#23966-1; CAS: 9002-98-6, 26913-06-4
Sodium butyrate	Aladdin	Cat#S102956; CAS:156-54-7
EDTA free Protease Inhibitor Cocktail	TargetMol	Cat#C0001
Lauryl maltose neopentyl glycol (LMNG)	Anatrace	Cat#NG310
Cholesteryl hemisuccinate tris salt (CHS)	Anatrace	Cat#CH210
Glycodiosgenin (GDN)	Anatrace	Cat#GDN101
POPS (16:0-18:1 PS)	Avanti	Cat#840034P
POPC (16:0-18:1 PC)	Avanti	Cat#850457P
Cholesterol	Sigma Aldrich	Cat#C8667; CAS:57-88-5
Bio-Beads SM-2 Resin	Bio-Rad	Cat#1523920
ATP	Sigma Aldrich	Cat#A2383
Methyl-β-cyclodextrin (M-βCD)	Sigma Aldrich	Cat#332615; CAS:128446-36-6
Dulbecco's modified eagle's medium (DMEM)	Gibco	Cat#11965092
Fetal bovine serum (FBS)	Gibco	Cat#10091148
Penicillin-Streptomycin (100X Solution)	Sangon Biotech	Cat#E607011
Lipofectamine™ 3000 Transfection Reagent	Invitrogen	Cat#L3000-075
[1,2-^{3}H(N)]-Cholesterol	PerkinElmer	Cat#NET139250UC
High density lipoprotein (HDL)	Sigma Aldrich	Cat#L8039; CAS:308068-14-6
Apolipoprotein A-I (apo A-I)	Sigma Aldrich	Cat#A0722
NON-Fat Powdered Milk	Sangon Biotech	Cat#A600669
7-Diethylamino-3-(4-maleimidophenyl)-4-methylcoumarin (CPM)	Invitrogen	Cat#76877-33-3
Bovine Serum Albumin (BSA)	Sangon Biotech	Cat#A500023-0100
Triton X-100	Thermo Scientific	Cat#85111
Tween-20	BBI Life Sciences	Cat#A600560-0500
Dimethyl Sulfoxide (DMSO)	Sigma Aldrich	Cat#20-139
DAPI	Sigma Aldrich	Cat#D9542
Antifade Mounting Medium	Vector Laboratories	Cat#H-1000
Critical commercial assays		
ATPase Activity Kit (Colorimetric)	Innova Biosciences	Cat#601-0120

(*Continued on next page*)

Continued

REAGENT or RESOURCE	SOURCE	IDENTIFIER
Deposited data		
Coordinates of human ABCG1, cholesterol-ATP-sphingomyelin bound	This paper	PDB: 7FDV
Cryo-EM map of human ABCG1, cholesterol-ATP-sphingomyelin bound	This paper	EMDB: EMD-31547
Experimental models: Cell lines		
HEK 293F	Invitrogen	Cat#R79007
HEK 293T	ATCC	Cat#CRL-11268
Recombinant DNA		
Codon-optimized human *ABCG1* (isoform 1)	GENEWIZ	N/A
Modified pcDNA3.1 vector suitable for expression in mammalian cells	This paper	N/A
pcDNA3.1-ABCG1(WT)-FLAG	This paper	N/A
pcDNA3.1-ABCG1(E242Q)-FLAG	This paper	N/A
pcDNA3.1-ABCG1(F467A)-FLAG	This paper	N/A
pcDNA3.1-ABCG1(L475F)-FLAG	This paper	N/A
pcDNA3.1-ABCG1(Q563A)-FLAG	This paper	N/A
pcDNA3.1-ABCG1(P570A)-FLAG	This paper	N/A
pcDNA3.1-ABCG1(V571A)-FLAG	This paper	N/A
pcDNA3.1-ABCG1(I574F)-FLAG	This paper	N/A
pcDNA3.1-ABCG1(H171A)-FLAG	This paper	N/A
pcDNA3.1-ABCG1(R213A)-FLAG	This paper	N/A
pcDNA3.1-ABCG1(S420A)-FLAG	This paper	N/A
pcDNA3.1-ABCG1(H424A)-FLAG	This paper	N/A
pcDNA3.1-ABCG1(F459A)-FLAG	This paper	N/A
pcDNA3.1-ABCG1(F460A)-FLAG	This paper	N/A
pcDNA3.1-ABCG1(F582A)-FLAG	This paper	N/A
pcDNA3.1-ABCG1(F582L)-FLAG	This paper	N/A
pcDNA3.1-ABCG1(F583A)-FLAG	This paper	N/A
pcDNA3.1-ABCG1(F583L)-FLAG	This paper	N/A
pcDNA3.1-ABCG1(S420A/H424A)-FLAG	This paper	N/A
Software and algorithms		
SerialEM	Mastronarde (2005)	https://bio3d.colorado.edu/SerialEM/
MotionCor2	Zheng et al. (2017)	https://msg.ucsf.edu/software
CTFFIND4	Rohou and Grigorieff (2015)	http://grigoriefflab.janelia.org/ctffind4
Relion 3.1	Scheres (2012)	https://github.com/3dem/relion
cryoSPARC	Punjani et al. (2017)	https://cryosparc.com
UCSF Chimera	Pettersen et al. (2004)	https://www.cgl.ucsf.edu/chimera
COOT	Emsley et al. (2010)	https://www2.mrclmb.cam.ac.uk/personal/pemsley/coot/
PHENIX	Adams et al. (2010)	https://phenix-online.org
PyMOL	PyMOL	http://www.pymol.org
ImageJ	Schneider et al. (2012)	https://imagej.nih.gov/ij/
OriginPro	N/A	https://www.originlab.com/Origin
Other		
Gold Mix (green)	Tsingke Biological Technology	Cat#TSE102
Quantifoil R1.2/1.3 300 mesh Au holey carbon grids	Quantifoil	Cat#X-101-Au300

(*Continued on next page*)

Continued

REAGENT or RESOURCE	SOURCE	IDENTIFIER
Superdex® 200 Increase 10/300 GL	GE Healthcare	Cat#GE28-9909-44
BeyoGel™ Plus Precast PAGE Gel (8 to 15%) for Tris-Gly System	Beyotime	Cat#P0472S
Unstained Protein MW Marker	Thermo Scientific	Cat#26610
ColorMixed Protein Marker	Beijing Solarbio Science & Technology	Cat#PR1920

RESOURCE AVAILABILITY

Lead contact

Further information and requests for reagents may be directed to and will be fulfilled by Yuxing Chen (cyxing@ustc.edu.cn), the lead contact.

Materials availability

This study did not generate new unique reagents.

Data and code availability

All relevant data are available from the authors and/or included in the manuscript or supplemental information. Atomic coordinates and EM density maps of the human ABCG1 in this paper (PDB: 7FDV; EMDB: EMD-31547) have been deposited in the Protein Data Bank and the Electron Microscopy Data Bank, respectively.

This paper does not report original code.

Any additional information required to reanalyze the data reported in this work paper is available from the lead contact upon request.

EXPERIMENTAL MODEL AND SUBJECT DETAILS

Cell culture

HEK 293F cells were cultured in SMM 293T-II medium (Sino Biological Inc.) at 37°C, supplemented with 5% CO_2. The cell transfection was manipulated when cell density reached ~2.5 × 10^6 cells per mL.

HEK 293T cells were maintained in Dulbecco's Modified Eagle's Medium (DMEM) (Invitrogen) supplemented with 10% (v/v) fetal bovine serum (FBS) (GibcoTM), at 37°C with 5% CO_2.

METHOD DETAILS

Protein expression and purification

The codon-optimized full-length human *ABCG1* gene was synthesized by GENEWIZ Company. The wild type was subcloned into a modified pcDNA3.1 vector with a linker (GTSGTSGTS) followed by a C-terminal FLAG tag (DYKDDDDK). Point mutations were introduced using a standard two-step PCR.

For 800 mL HEK 293F cell culture, ~2 mg plasmids premixed with 4 mg linear polyethylenimines (PEIs) (Polysciences, Inc) in 45 mL fresh medium for 15 min, then the mixture and another 150 mL fresh medium were added into cell culture, followed by 30-min static incubation. The transfected cells were grown at 37°C for 12~16 hr, then 10 mM sodium butyrate (Aladdin) was added, and cultured at 30°C for additional 48 hr before harvesting. After centrifugation at 4,000 *g* for 5 min, the cell pellets were resuspended in the lysis buffer containing 30 mM Tris-HCl pH 7.5, 150 mM NaCl, 20% glycerol (v/v), 2 mM $MgCl_2$, 7 mM β-Mercaptoethanol (β-ME) and ethylenediaminetetraacetic acid (EDTA) free protease inhibitor cocktail (TargetMol). The suspension was frozen in liquid nitrogen and stored at -40°C for further use.

For membrane solubilization and protein extraction, the thawed suspension was incubated in the lysis buffer with additional 1% (w/v) lauryl maltose neopentyl glycol (LMNG, Anatrace), 0.1% (w/v) cholesteryl hemisuccinate (CHS, Anatrace) with gentle rotation at 8°C for 2.5 h. After ultracentrifugation at 45,000 rpm for 45 min (Beckman, Type 70 Ti), the supernatant was incubated with the anti-FLAG M2 affinity gel (Sigma Aldrich) at 8°C for 1 hr. Then the resin was loaded onto the column and washed six times, each with 5 mL of wash buffer A containing 30 mM Tris-HCl pH 7.5, 150 mM NaCl, 10% glycerol (v/v), 2 mM $MgCl_2$, 0.03% (w/v) glycodiosgenin (GDN, Anatrace). Protein was eluted with 6 mL of wash buffer B containing 30 mM Tris-HCl pH 7.5, 150 mM NaCl, 5% glycerol (v/v), 2 mM $MgCl_2$, 0.02% (w/v) GDN plus 200 μg/mL FLAG peptide. The eluent was concentrated by a 100-kDa cut-off Centricon (Millipore) and then applied to size-exclusion chromatography (Superdex® 200 Increase 10/300, GE Healthcare) in wash buffer C containing 30 mM Tris-HCl pH 7.5, 150 mM NaCl, 2 mM $MgCl_2$, 0.02% (w/v) GDN. Peak fractions were pooled and frozen in liquid nitrogen or concentrated for EM analysis. For nanodiscs reconstruction, 0.02% GDN was substituted by 0.01% LMNG (w/v), and 0.001% CHS (w/v) during purification.

Nanodiscs preparation

For nanodiscs preparation, concentrated ABCG1 solubilized in LMNG/CHS was reconstituted into lipid nanodiscs by mixing the ABCG1 with purified MSP1D1 scaffold protein and a LMNG/CHS (0.5%, w/v) solubilized mixture (w/w) of 60% 1-palmitoyl-2-oleoyl-glycero-3-phosphocholine (POPC, Avanti) and 20% 1-palmitoyl-2-oleoyl-sn-glycero-3-phospho-L-serine (POPS, Avanti) plus 20% cholesterol (Sigma Aldrich) or 75% POPC and 25% POPS at a molar ratio of 2:3:150. After incubation of the mixture at 4°C for 1 hr, 0.7 g/mL of biobeads SM-2 were added and the mixture was gently rotated overnight at 14°C to remove detergent. The following day, the biobeads were removed and the collected ABCG1 nanodiscs were injected over a Superdex® 200 Increase gel filtration column in buffer N containing 30 mM Tris (pH 7.5), 150 mM NaCl. Peak fractions were pooled and concentrated to ~0.5 mg/mL for biochemical studies.

ATPase activity assay

ATPase activities of recombinant wild-type ABCG1 and mutants in the nanodiscs were measured using the ATPase colorimetric Assay Kit (Innova Biosciences).

Reactions were performed at 37°C for 45 min and the amount of released Pi was quantitatively measured using SpectraMax iD5 Multi-Mode Microplate Reader (Molecular Devices) in 96-well plates at $OD_{650\ nm}$.

Lipid purification and mass spectrometry

Lipids in these samples were purified by Bligh–Dyer isolation. The protein samples were converted to one phase solution of buffer/chloroform/methanol (0.8:1:2, v/v/v). After being incubated at room temperature for 30 min, the suspension was converted into a two-phase Bligh–Dyer system buffer/chloroform/methanol (1.8:2:2, v/v/v) by addition of buffer and methanol. After mixing thoroughly and centrifugation at 3000 g for 5 min, the lower phase was collected and used for mass spectrometry analysis. Accurate mass measurements were acquired using an Agilent 6545 QTOF mass spectrometer. The parameters used for the mass spectrometer with ESI-negative mode were as follows: capillary voltage of 2.5 kV, nozzle voltage of 1000 V, gas temperature of 320°C, drying gas of 8 L/min, nebulizer pressure of 35 psi, sheath gas temperature of 350°C, sheath gas of 11 L/min. The mass spectrometer was operated both in MS mode and MS/MS mode, of which the collision energy is 20 or 30 eV. Scan range was from m/z 100 to 1000.

Cellular cholesterol efflux assay

The cellular cholesterol efflux assays were performed according to the previous report (Wang et al., 2004) with minor modifications. Briefly, HEK 293T cells were seeded on 24-well collagen-coated BioCoat plates (Corning) and transfected at approximately 75% confluency with Lipofectamine 3000 (Invitrogen) and plasmid according to the manufacturer's protocols. Transfected HEK293T cells were labeled by culturing for 24 hr in 10% FBS/DMEM containing 0.5 μCi/mL [^{3}H]cholesterol (PerkinElmer, Inc) for cholesterol efflux. Then, the cells were washed and equilibrated overnight in serum-free medium. The next day, the cells were washed, then apoA-I (final concentration 10 μg/ml), HDL (final concentration 20 μg/ml) or M-βCD (final concentration 200 μg/ml) were added as acceptor and incubated in fresh serum-free medium for 4 hr before the medium and cells were collected for analysis. After washing with fresh media, cells were lysed with 0.1% SDS and 0.1 M NaOH lysis buffer, and radioactivity was determined by Tri-Carb 2910TR liquid scintillation counter (PerkinElmer, Inc). Cholesterol efflux was expressed as the percentage of the radioactivity released from the cells into the medium relative to the total radioactivity in cells plus medium. The expression of ABCG1 mutants in HEK 293T cells for cellular cholesterol efflux were tested by western blotting. Expressions of variants M471F and F567A were non-detectable, which were thus excluded from the assay data.

Western blot analysis

The whole cell lysate samples were run on BeyoGel™ Plus Precast PAGE Gel (8 to 20%) for Tris-Gly System (Beyotime) for 110 min at 110 V. Gels were transferred to PVDF membranes with the Trans-Blot Turbo Transfer System (BIO-RAD). The membranes were blocked by 5% (w/v) non-fat milk (Sangon Biotech) at 4°C overnight, before incubation with primary antibody for 1 hr at ambient temperature. Then the membranes were washed 3 times with TBST buffer before incubation with secondary antibody for 45 min at ambient temperature. The membranes were washed 3 times and imaged via ImageQuant LAS4000 (Cytiva). For semiquantitative analysis, band intensities were measured by densitometry using the software ImageJ.

Primary antibodies used in this study include: FLAG tag mouse monoclonal antibody (1:3,000, Proteintech) and β-actin mouse monoclonal antibody (1:40,000, Proteintech). Secondary antibody used in this study is HRP-conjugated Affinipure Goat Anti-Mouse IgG (H+L) (1:10,000, Proteintech).

Cryo-EM sample preparation and data collection

The purified $ABCG1_{E242Q}$ mutant was concentrated to approximately 3.5 mg/mL and incubated with 10 mM Mg^{2+}/ATP for 15 min. An aliquot of 3.5 μL of the sample was applied to glow-discharged Quantifoil R1.2/1.3 300-mesh Au Holey Carbon Grids. The grids were blotted for 4 s with the blot force 0, and then plunged into liquid ethane using a Vitrobot Mark IV (FEI) at 8°C and 100% humidity.

Images were collected in super resolution mode under a 300 keV Titan Krios electron microscope (FEI), equipped with K2 Summit direct electron detector (Gatan) at a nominal magnification of 29,000× with a defocus range from -2.0 to -1.2 μm, using Serial EM (Mastronarde, 2005). A total of 9,071 micrograph stacks were collected from three individual grids with the E242Q mutant sample.

Each stack was recorded for 5.76 s with 32 frames. The electron dose rate is 10 $e^{-}/Å^2/s$ and the resulting total dose is ~57.6 $e^{-}/Å^2$. The stacks were motion corrected and dose weighted using MotionCor2 (Zheng et al., 2017), binned 2-fold to yield a pixel size of 1.01 Å. The defocus values were estimated using CTFFIND4 (Rohou and Grigorieff, 2015).

Image processing

A total of 3,537,774 particles were automatically picked from 9,071 micrographs. These particles were then subjected to reference-free 2D classification and particles of the best classes were re-extracted for further data processing. A total of 3,038,114 particles were subjected to initial model building and further global angular searching 3D classification in RELION3.1 (Scheres, 2012). Several rounds of global angular searching 3D classification with C2 symmetry was performed, during which particles were classified into 4 classes. Particles from the best classes were merged together and subjected to local angular searching 3D classification. The 3D auto-refinement of the 274,879 selected particles generated an EM map with an overall resolution of 4.4 Å. By particle re-extracting and applying a soft mask during refinement, the resolution was improved to 3.84 Å. These particles were selected and subtracted with a mask excludes the signal of detergent micelles, then imported into cryoSPARC3.2 (Punjani et al., 2017) for *ab-initio* reconstruction and heterogeneous refinement requesting 4 classes. 151,593 particles from the best class were further subjected to non-uniform refinement and local refinement, resulting in a final map at 3.26 Å resolution.

Map resolutions were estimated with the gold-standard Fourier shell correlation 0.143 criterion (Rosenthal and Henderson, 2003) (Figure S2C).

Model building and refinement

To assist model building, the working map was sharpened with a B-factor of -142 $Å^2$. A homology model of ABCG1 was generated by the SWISS-MODEL server, using the EM structure of human ABCG2-MXN (PDB: 6VXI) as the reference. The model was docked into the 3.26 Å map of ABCG1 using Chimera (Pettersen et al., 2004). Each residue was manually adjusted with Coot (Emsley and Cowtan, 2004). Structure refinements were carried out by Phenix (Adams et al., 2010) in real space with secondary structure and geometry restraints to prevent structure overfitting. The geometries of the model were validated using MolProbity (Chen et al., 2010; Davis et al., 2007). Refinement statistics of the model are given in Table S1. Figures were prepared using UCSF Chimera (Pettersen et al., 2004), ChimeraX (Pettersen et al., 2021) or PyMOL (https://pymol.org).

Immunofluorescence

HEK 293T cells were transfected with ABCG1-FLAG and mCherry tagged organelles as indicated. Transfection of plasmids into cells was performed with Lipofectamine 3000 (Invitrogen) according to the user manual. Cells grown on coverslips were fixed with PBS supplemented with 3.7% paraformaldehyde at 37°C. The fixed cells were permeabilized with 0.1% Triton X-100 (Thermo Fisher Scientific) and blocked with 1% BSA (Sigma Aldrich). The cells were then incubated with rabbit-anti-FLAG antibody (Sigma Aldrich) and FITC conjugated goat-anti-rabbit antibody (Jackson ImmunoResearch). DAPI dye was to show cell nucleus. Images were captured by DeltaVision softWoRx software (Applied Precision) and processed by deconvolution and z-stack projection.

Microscale fluorescent thermal stability assay

The thermal stability assay was performed using a previously described technique with slight modification (Alexandrov et al., 2008). CPM dye (Invitrogen) was dissolved in DMSO (Sigma) at 4 mg/ml. This stock solution was kept at −80°C. Prior to use, the dye stock is diluted 1:100 in dye dilution buffer (30 mM Tris-HCl pH 7.5, 150 mM NaCl, 0.01% LMNG and 0.001% CHS), and is used immediately while protected from light to reduce photobleaching. The thermal denaturation assay was performed in a total volume of 30 μL. The purified samples of ABCG1 variants (10 μg) was diluted in the dye dilution buffer to a final volume of 24 μL. Then, 6 μL of the diluted dye was added and thoroughly mixed with the protein samples. The reaction mixture was heated in a controlled manner with a ramp rate of 6°C/min in a LightCycler® 480 System (Roche). The excitation wavelength was set at 440 nm, and the emission wavelength was 488 nm. Assays were performed over a temperature range starting from 37°C and ending at 80°C.

QUANTIFICATION AND STATISTICAL ANALYSIS

To quantify the ATPase activity, the cholesterol efflux efficiency and the expression level, mean values and the standard deviation from at least three independent measurements were calculated. The half maximum effective concentration of cholesterol and the maximum ATPase activity of ABCG1 were determined by nonlinear regression of the Michaelis-Menten equation using OriginPro. The specific ATP turnover rates were calculated assuming a molecular weight of 152 kDa for ABCG1 homodimer.

The orientation distribution of the particles used in the final reconstruction and the local resolution map was calculated using cryoSPARC3.2. Resolution estimations of cryo-EM density maps are based on the 0.143 Fourier shell correlation criterion (Kucukelbir et al., 2014).

The multiple sequence alignments were performed by MultAlin (http://multalin.toulouse.inra.fr/multalin/) (Corpet, 1988).